LONG-WAVELENGTH 256X256 GaAs/AlGaAs QUANTUM WELL INFRARED PHOTODETECTOR (QWIP) PALM-SIZE CAMERA

S. D. Gunapala, S. V. Bandara, J. K. Liu, E. M. Luong, M. J. McKelvey, J. M. Mumolo, S. B. Rafol, C. A. Shott, and N. Stetson

ABSTRACT

A 9 μm cutoff 256x256 palm-size quantum well infrared photodetector (QWIP) camera weighing only 2.5 pounds and using 5.5 Watts of power has been demonstrated. Excellent imagery, with a noise equivalent differential temperature (NE T) of 23 mK has been achieved. It is well known that QWIP has very low 1/f noise. As a result, this camera uses a pre-recorded non-uniformity correction table (i.e., gains and offsets) stored in its read-only-memory during operation. In this paper, we discuss the development of this very sensitive long-wavelength infrared (LWIR) camera based on a GaAs/AlGaAs QWIP focal plane array (FPA) and its performance in terms of quantum efficiency, NE T, MRDT, uniformity, and operability.

This was jointly sponsored by the Ballistic Missile Defense Organization / Innovative Science & Technology Office, and the National Aeronautics and Space Administration, Office of Space Science.

S. D. Gunapala, S. V. Bandara, J. K. Liu, E. M. Luong, M. J. McKelvey, J. M. Mumolo, and S. B. Rafol are with Center for Space Microelectronics Technology, Jet Propulsion Laboratory, California Institute of Technology, Pasadena, CA 91109.

C. A. Shott with Amber, A Raytheon Company, Goleta, CA 93117.

N. Stetson with Inframetrics, Inc., 16 Esquire Road, No. Billerica, MA 01862

I. INTRODUCTION

NASA, commercial, medical, and defense applications such as Earth observation systems, astronomy, weather monitoring, thermal mapping, thermography, missile tracking, and night vision aids, etc. require high performance large format long-wavelength infrared (LWIR) detector arrays in the wavelength range of 8-16μm. Thus, NASA and Ballistic Missile Defense Organization (BMDO) have devoted a significant effort in developing highly sensitive infrared detectors and large format focal plane arrays (FPAs) based on novel "artificial" low "effective" band-gap semiconductor material systems such as GaAs/AlGaAs [1,2]. Caltech, Jet Propulsion Laboratory (JPL) under contract from NASA and BMDO has extensively pursued GaAs/AlGaAs based multi-quantum wells (MQWs) for infrared radiation detection. Through the optimization of the detector design, light coupling schemes and development of large format FPA fabrication and packing, portable 256x256 QWIP FPA infrared cameras have been realized [3-5]. Similarly, a TV format (i.e., 640x486) QWIP camera which can see 8.5 μm has been demonstrated [6]. These achievements bring forth great promise for myriad applications in the 6-20 μm wavelength region [7]. In this paper we discuss fabrication, characterization, and performance of the 256x256 LWIR QWIP FPA and demonstration of the palm-size LWIR camera based on this 256x256 FPA.

Improving QWIP performance depends largely on minimizing the dark current that plagues all light detectors (i.e., the current that flows through a biased detector in the dark with no photons impinging on it). As we have discussed elsewhere [2], at temperatures above 45 K, the dark current of the LWIR (<10 μm) QWIP is mostly dominated by classic thermionic emission of ground state electrons directly out of the well into the energy continuum [8]. Minimizing this last component is critical to the commercial success of the QWIP as it allows the highly desirable high temperature FPA operation.

II. TEST STRUCTURE RESULTS

We have designed the bound-to-quasibound quantum well by placing the first excited state exactly at the well top as described elsewhere [2]. Each period of the MQW structure consists of a 45 Å well of GaAs (doped n = $4x10^{17}$ cm^{-3}) and a 500 Å barrier of $Al_{0.3}Ga_{0.7}As$. Fifty such periods are stacked together for higher photon absorption (See Fig. 1). Ground state electrons are provided in the detector by doping the GaAs well layers with Si. This photosensitive MQW structure is sandwiched between 0.5 μm GaAs top and bottom

contact layers doped n = $4x10^{17}$ cm^{-3}, grown on a semi-insulating GaAs substrate by molecular beam epitaxy (MBE). Then a 0.7 μm thick GaAs cap layer on top of a 300 Å $Al_{0.3}Ga_{0.7}As$ stop-etch layer is grown *in situ* on top of the device structure to fabricate the light coupling optical cavity. The MBE grown QWIP structure is processed into 200 μm diameter mesa test structures (area = 3.14 x 10^{-4} cm^2) using wet chemical etching, and Au/Ge ohmic contacts are evaporated onto the top and bottom contact layers.

The detectors are back illuminated through a 45° polished facet [2] and a responsivity spectrum is shown in Fig. 2. The responsivity of the detector peaks at 8.4 μm and the peak responsivity (R_p) of the detector is 168 mA/W at bias V_B = -2 V. The spectral width and the cutoff wavelength are λ/λ = 10% and λ_c = 8.8 μm respectively. The measured absolute peak responsivity of the detector is small, from V_B = 0 to -0.5 V. Beyond that it increases nearly linearly with bias reaching R_P = 365 mA/W at V_B = -5 V. This type of behavior of responsivity versus bias is typical for a bound-to-quasibound QWIP. The peak quantum efficiency was 16.6% at bias V_B = -2 V for a 45° double pass. The lower quantum efficiency is due to a lower well doping density ($4x10^{17}$ cm^{-3}) as it is necessary to suppress the dark current for the highest possible operating temperature. A peak quantum efficiency as high as 25% has already been achieved with regular well doping density (i.e., $1x10^{18}$ cm^{-3}). Due to lower readout multiplexer well depth (i.e., $5x10^6$ electrons), a lower dark current is mandatory to achieve a higher operating temperature. In this case, the highest operating temperature of 74 K was determined by the cooling capacity of the small integral Sterling cooler used in an Inframetric's *InfraCAM* ™ camera.

The photoconductive gain g was experimentally determined using $g = i_n^2 / 4eI_DB$, where B is the measurement bandwidth, and i_n is the current noise, which was measured using a spectrum analyzer. The photoconductive gain of the detector reached 0.32 at V_B =-5 V. The peak detectivity is defined as $D_p^* = R_p\sqrt{AB} / i_n$, where R_P is the peak responsivity, A is the area of the detector and A = $3.14x10^{-4}$ cm^2. The measured peak detectivity at bias V_B = -2.0 V and temperature T = 70 K is $2.0x10^{11}$ cm Hz/W. Figure 3 shows the bias dependence of peak detectivity at temperatures 70, 75 and 80 K. These detectors show background limited performance (BLIP) at bias V_B = -2 V and temperature T = 72 K for 300 K background with f/2 optics.

III. IMAGING ARRAYS

It is well known that GaAs/AlGaAs based n-type QWIPs do not absorb infrared radiation incident normal to the surface. Thus, researchers have invented various light coupling schemes such as two-dimensional (2-D) periodic gratings [9], random reflectors [10], corrugated reflectors [11], lattice mis-match strain material systems, and p-type materials [2, 12]. Many of our previous FPAs utilized random reflectors for efficient light coupling. Although random reflectors have achieved relatively high quantum efficiencies with large test device structures, it is not possible to achieve the similar high quantum efficiencies with random reflectors on small FPA pixels due to the reduced width-to-height aspect ratios. In addition, it is difficult to fabricate random reflectors for shorter wavelength detectors relative to very long-wavelength detectors (i.e., 15 μm) due to the fact that feature sizes of random reflectors are linearly proportional to the peak wavelength of the detectors. For example, the minimum feature size of random reflectors of 15 μm cutoff and 9 μm cutoff FPAs were 1.25 and 0.6 μm respectively, and it is difficult to fabricate sub-micron features by contact photolithography. As a result, the random reflectors of the 9 μm cutoff FPA were less sharp and had fewer scattering centers compared to the random reflectors of the 15 μm cutoff QWIP FPA. Thus, 2-D periodic grating structure is used for efficient light coupling into QWIPs. As we have discussed before [2], two passes of infrared radiation can be coupled to the QWIP detector structure by incorporating a two dimensional grating surface [9] on top of the detectors. This 2-D periodic grating structure is fabricated on the detectors by using standard photolithography and SF_6:BCl_3 selective dry etching.

After the 2-D grating array (calculations of the 2-D grating parameters and light coupling experiments were extensively discussed in references 2 and 9) was defined by the photolithography and dry etching, the photoconductive QWIPs of the 256x256 FPAs were fabricated by wet chemical etching through the photosensitive GaAs/$Al_XGa_{1-X}As$ MQW layers into the 0.5 μm thick doped GaAs bottom contact layer. The pitch of the FPA is 38 μm and the actual pixel size is 28x28 μm^2. The 2-D grating reflectors on top of the detectors were then covered with Au/Ge and Au for Ohmic contact and reflection. Twenty five QWIP FPAs were processed on a 3-inch GaAs wafer. Indium bumps were then evaporated on top of the detectors for silicon readout circuit (ROC) hybridization. A single QWIP FPA was

chosen and hybridized (via an indium bump-bonding process) to a 256x256 CMOS multiplexer (Amber AE-166).

The gaps between FPA detectors and the readout multiplexer were backfilled with epoxy. This epoxy backfilling provides the necessary mechanical strength to the detector array and readout hybrid prior to the thinning process. Substrate thinning (or substrate removal) is very important for the success of cryogenic FPA hybrids. During the first step of the thinning process, an approximately 500 μm thick GaAs layer was removed using abrasive polishing or diamond turning (See Fig. 4). Then Bromine-Methanol chemical polishing was used to remove another approximately 100 μm thick GaAs layer. This step is very important because it removes all scratch marks left on the substrate due to abrasive polishing. Otherwise these scratch marks will be enhanced and propagated in to the final step via preferential etching. Then, wet chemical etchant was used to reduce the substrate thickness to several microns and then SF_6:BCl_3 selective dry etchant was used as the final etch. This final etching completely removed the remaining GaAs substrate. At this point the remaining GaAs/AlGaAs material contains only the QWIP pixels and a very thin membrane (~1000Å). The thermal mass of this membrane is insignificant compared to the rest of the hybrid. This allows it to adapt to the thermal expansion and contraction coefficients of the silicon readout multiplexer and completely eliminates the thermal mis-match problem between the silicon based readout and the GaAs based detector array. This basically allows QWIP FPAs to go through an unlimited number of temperature recycles without any indium bump breakage and peeling-off. Furthermore, this substrate removal process provides two additional advantages for QWIP FPAs: those are the complete elimination of pixel-to-pixel optical cross-talk and a significant (a factor of two with 2-D periodic gratings) enhancement in optical coupling of infrared radiation into QWIP pixels [2].

One selected 256x256 QWIP FPA hybrid was mounted on to the cold finger of a liquid nitrogen cooled laboratory test dewar and biased at V_B =-2V. Temperature of the dewar was lowered by pumping on liquid nitrogen. This selected FPA was tested at temperatures 65, 70, and 75 K. At temperatures below 72 K, the signal to noise ratio of the system is limited by array non-uniformity, multiplexer readout noise, and photo current noise (for f/2 optics). At temperatures above 72 K, temporal noise due to the QWIP's higher dark current becomes the limitation. As mentioned earlier this higher dark current is due to thermionic emission and thus causes the charge storage capacitors of the readout circuitry to saturate. Since the QWIP is a high impedance device, it yields a very high charge injection coupling efficiency into the integration capacitor of the multiplexer. The differential

resistance R_{Det} of the pixels at -2 V bias is 3.0×10^{10} Ohms at T=70 K and detector capacitance C_{Det} is 3.0×10^{-14} F. The detector dark current I_{Det} = 24 pA under the same operating conditions. Charge injection efficiency into the the CMOS readout multiplexer was calculated as described in reference [13] and [14]. The calculated charge injection efficiency exceeds 90% at a 60 Hz frame rate. The FPA was back-illuminated through the flat thinned substrate membrane (thickness $\approx$ 1000 Å). This FPA gave excellent images with 99.87% of the pixels working (number of dead pixels $\approx$ 88) , demonstrating the high yield of GaAs technology. The operability is defined as the percentage of pixels having noise equivalent differential temperature less than 100 mK at a 300 K blackbody.

In the following test, the background temperature T_B was 300 K, the area of the pixel A = $(28\ \mu m)^2$, the f number of the optical system is 2, and the frame rate is 60 Hz. Figure 5 shows the measured NE T of the FPA at an operating temperature of T = 70 K, bias V_B = -2 V for 300 K background and the mean value is 23 mK. The uncorrected NE T nonuniformity (sigma/mean) is 5.4%. This agrees reasonably with our estimated value of 8 mK based on test structure data. The peak quantum efficiency of the FPA is 5.7% (lower FPA quantum efficiency is attributed to 54% fill factor, 30% substrate reflection and 90% charge injection efficiency) and this corresponds to an average of two passes of infrared radiation (equivalent to a single 45° pass) through the photosensitive MQW region. Figure 6 shows the quantum efficiency histogram of the FPA, and the uncorrected nonuniformity (sigma/mean) is 5.5%.

IV. PALM-SIZE CAMERA

A 256x256 QWIP FPA hybrid was mounted onto a 130 mW integral Sterling closed-cycle cooler assembly and installed into an Inframetric's *InfraCAM*™ camera-body, to demonstrate a palm-size LWIR camera (shown in Fig. 7). The camera is equipped with a 50 mm focal length f/1.3 germanium lens with an 11.2 degree field of view designed to be transparent in the 8-12 μm wavelength range to be compatible with the QWIP's 8.5 μm operation. The dimensions of the camera are 5.3"x 9.7"x 2.5" and it weighs less than three pounds including battery, lens, and viewfinder. The lens assembly can easily be removed, and other lenses can be attached to provide other fields of view or higher resolution images. The power consumption of the camera is 5.5 Watts and it runs more than two hours with a 2400 mAh, 6-Volt camcorder battery.

The measured mean NE T of the QWIP *InfraCAM*™ is 38 mK at an operating temperature of T = 74 K and bias V_B = -2 V, for a 300 K background (the higher NE T is mostly due to the higher operating temperature). Figure 8 shows the DC signal histogram before two-point correction. It is worth noting that all uncorrected nonuniformities (NE T, quantum efficiency, and DC signal) of the 65,536 pixels of the 256x256 FPA are about 5.5% (= sigma/mean). The nonuniformity after two-point (17° and 27° Celsius) correction improves to an impressive 0.03% (See Fig. 9). As mentioned earlier, this high yield is due to the excellent GaAs growth uniformity and the mature GaAs processing technology. The dead pixel scatter of the FPA is shown in Fig. 10. Pixels having NE T>100 mK are counted as dead pixels, thus, the operability of this FPA is 99.87%. However, the actual number of dead pixels (i.e., no photo response) is less than 10, thereby making pixel replacement software unnecessary. It should be noted that this particular FPA is far from optimum and it does not represent the best nonuniformity and operability. The lowest uncorrected nonuniformities achieved in QWIP FPAs are 2% and the highest operabilities are >99.9%.

It is important to mention that this palm-size LWIR camera does not require any calibrations or nonuniformity corrections prior to data acquisition. Instead, it uses a nonuniformity correction table (i.e., gains and offsets) stored in its read-only-memory (ROM) for its entire life. It is worth noting that this technique is successful solely due to the higher stability (or lower 1/f noise) of QWIP FPAs. In other words, the nonuniformities of QWIP FPAs are almost independent of time. The minimum resolvable temperature difference was measured by two observers. While the collection of the data does not adhere to the generally accepted requirements of having multiple observers, the data is consistent with the NE T measurement and worth reporting. Data was taken with four-bar targets ranging in spatial frequency from 0.1 cycles/milli radian up to 0.9 cy/mr, the first target where no contrast could be measured (unclear). At the lowest spatial frequency, the MRDT was 10 mK (or 10 mCelsius). Figure 11 shows MRTD plotted as a function of the spatial frequency cy/mr.

Video images were taken at a frame rate of 60 Hz at temperatures as high as T = 74 K using a ROC capacitor having a charge capacity of 8×10^6 electrons (the maximum number of photoelectrons and dark electrons that can be counted in the time taken to read each detector pixel). Figure 12 shows one frame of a video image taken with a 9 μm cutoff 256x256 QWIP camera. This image demonstrates the high sensitivity of the 256x256 QWIP *InfraCAM* ™. The readout multiplexer used was a photovoltaic InSb multiplexer which was not optimized to supply the proper bias and impedance levels required by photoconductive

QWIPs. Implementation of these improvements should significantly enhance the QWIP FPA operating temperature (i.e., 80 K for 9 μm).

ACKNOWLEDGMENTS

The research described in this paper was performed by the Center for Space Microelectronics Technology, Jet Propulsion Laboratory, California Institute of Technology.

REFERENCES

1. Walter R. Dyer and Dwight Duston, Long Wavelength Infrared detectors and Arrays: Physics and Applications V, **97-33**, 1 (1997).
2. S. D. Gunapala and K. M. S. V. Bandara, Physics of Thin Films, Academic Press, **21**, 113 (1995).
3. S. D. Gunapala, J. K. Liu, J. S. Park, M. Sundaram, C. A. Shott, T. Hoelter, T. L. Lin, S. T. Massie, P. D. Maker, R. E. Muller, and G. Sarusi, IEEE Trans. Electron Devices **44**, 51 (1997).
4. R. Breiter, W. Cabanski, R. Koch, W. Rode, and J. Ziegler, SPIE **3379**, 423 (1998).
5. J. Y. Andersson, J. Alverbro, J. Borglind, P. Helander, H. Martijn, and M. Ostlund, SPIE **3061**, 740 (1997).
6. S. D. Gunapala, S. V. Bandara, J. K. Liu, W. Hong, M. Sundaram, P. D. Maker, R. E. Muller, C. A. Shott, and R. Carralejo, IEEE Trans. Electron Devices **45**, 1890 (1998).
7. S. D. Gunapala, S. V. Bandara, J. K. Liu, W. Hong, E. M. Luong, J. M. Mumolo, M. J. McKelvey, D. K. Sengupta, A. Singh, C. A. Shott, R. Carralejo, P. D. Maker, J. J. Bock, M. E. Ressler, M. W. Werner, and T. N. Krabach, SPIE **3379**, 382 (1998).
8. K. K. Choi, L. Fotiadis, M. Taysing-Lara, and W. Chang, Appl. Phys. Lett. **59**, 3303 (1991).
9. J. Y. Andersson, L. Lundqvist, and Z. F. Paska, Appl. Phys. Lett. **58**, 2264 (1991).
10. G. sarusi, B. F. Levine, S. J. Pearton, K. M. S. V. Bandara, and R. E. Leibenguth, Appl. Phys. Lett. 64, 960 (1994).
11. K. K. Choi, A. C. Goldberg, N. C. Das, M. D. Jhabvala, R. B. Bailey, and K. Vural, SPIE **3287**, 118 (1998).
12. S. S. Li and Y. H. Wang, Quantum Well Intersubband Transition Physics and Devices, NATO ASI Series, Kluwer Academic, **270**, 29 (1994).
13. C. G. Bethea, B. F. Levine, M. T. Asom, R. E. Leibenguth, J. W. Stayt, K. G. Glogovsky, R. A. Morgan, J. D. Blackwell, and W. J. Parrish, "Long Wavelength Infrared 128 x 128 AlxGa1-xAs/GaAs Quantum Well Infrared Camera and Imaging System," *IEEE Trans. Electron. Devices*, vol. 40, pp. 1957-1963, 1993.
14. L. J. Kozlowski, G. M. Williams, G. J. Sullivan, C. W. Farley, R. J. Andersson, J. Chen, D. T. Cheung, W. E. Tennant, and R. E. DeWames, "LWIR 128x128 GaAs/AlGaAs Multiple Quantum Well Hybrid Focal Plane Array," *IEEE Trans. Electron. Devices* , vol. ED-38, pp. 1124-1130, 1991.

FIGURE CAPTIONS

Fig. 1 Layer structure of the QWIP device used in this demonstration.

Fig. 2 Responsivity spectrum of a bound-to-quasibound LWIR QWIP test structure at temperature T = 77 K. The spectral response peak is at 8.5 μm and the long wavelength cutoff is at 8.9 μm.

Fig. 3 Detectivity as a function of bias voltage at temperatures T = 70 and 77 K.

Fig. 4 This figure shows the substrate removal process. During the first step of thinning process an approximately 500 μm thick GaAs layer is removed using abrasive polishing or diamond turning. Then Bromine-Methanol chemical polishing is used to remove another approximately 100 μm thick GaAs layer. In the third step, wet chemical etchant is used to reduce the substrate thickness to several microns. Then, SF_6:BCl_3 selective dry etchant is used as the final etch. This final etching completely removes the remaining GaAs substrate.

Fig. 5 Uncorrected noise equivalent differential temperature (NE T) histogram of the 65,536 pixels of the 256x256 array showing the uniformity of the FPA. The lowest QWIP FPA nonuniformity achieved is <2%. The uncorrected non-uniformity (= standard deviation/mean) of the FPA is only 5.4% including 1% non-uniformity of ROC and 1.4% non-uniformity due to the cold-stop not being able to give the same field of view to all the pixels in the FPA.

Fig. 6 Uncorrected quantum efficiency histogram of the 65,536 pixels of the 256x256 array showing a high uniformity of the FPA.

Fig. 7 Picture of 256x256 palm-size long-wavelength QWIP *InfraCAM* ™.

Fig. 8 Uncorrected DC signal histogram of the 65,536 pixels of the 256x256 array showing the high uniformity of the FPA.

Fig. 9 Residual DC signal histogram of the 65,536 pixels of the 256x256 array after two point correction. The corrected non-uniformity (= standard deviation/mean) of the FPA is only 0.03% .

Fig. 10 Dead pixel scatter. Pixels having NE T>100 mK are counted as dead pixels. Thus, the operability of this FPA is 99.87%. However, the actual number of dead pixels (i.e., no photo response) is less than 10.

Fig. 11 Minimum resolvable temperature difference (MRTD) plotted as a function of the spatial frequency.

Fig. 12 One frame of video image taken with the 9 μm cutoff 256x256 QWIP *InfraCAM* ™.

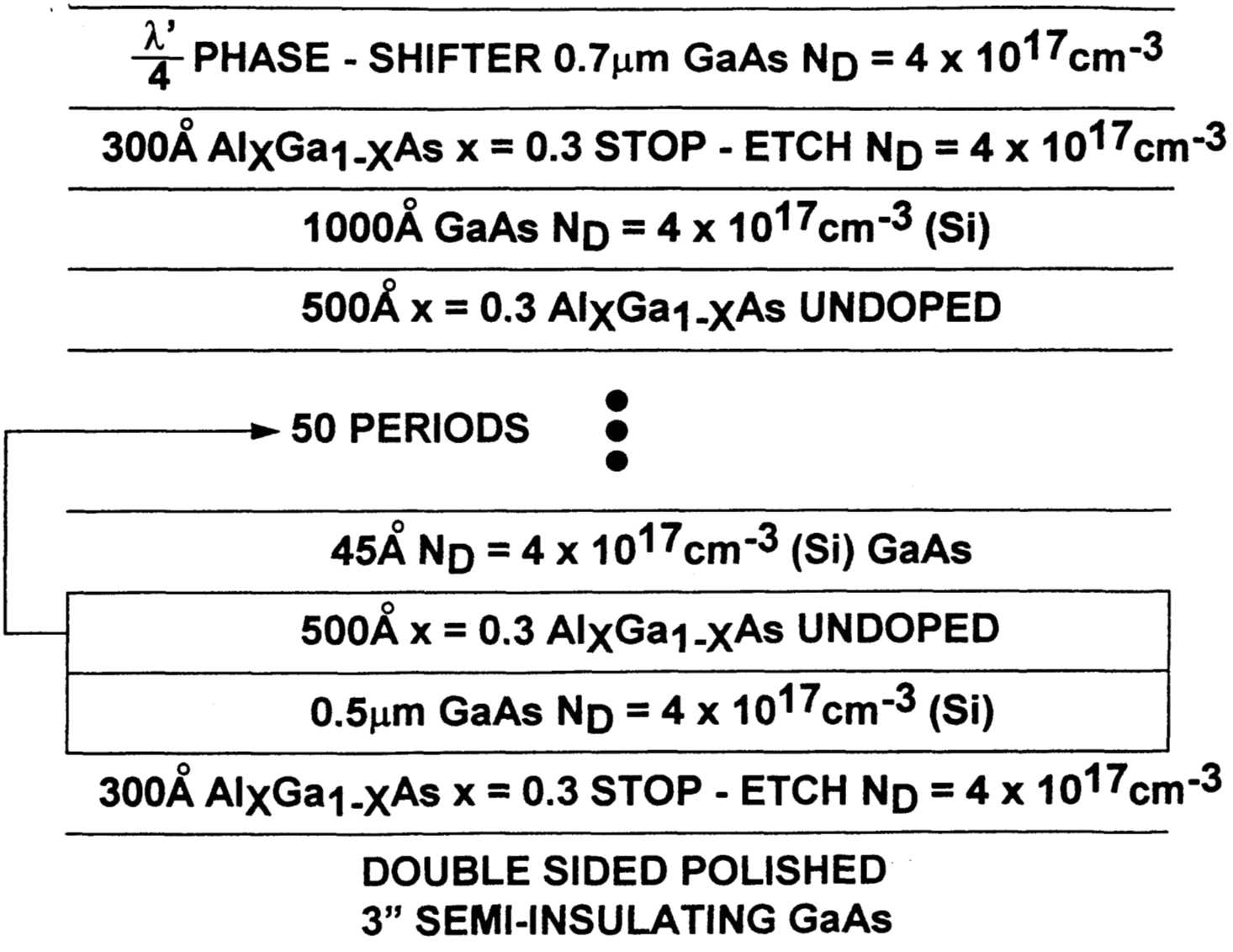
$\frac{\lambda'}{4}$ PHASE - SHIFTER 0.7μm GaAs $N_D = 4 \times 10^{17} cm^{-3}$
300Å $Al_XGa_{1-X}As$ x = 0.3 STOP - ETCH $N_D = 4 \times 10^{17} cm^{-3}$
1000Å GaAs $N_D = 4 \times 10^{17} cm^{-3}$ (Si)
500Å x = 0.3 $Al_XGa_{1-X}As$ UNDOPED
50 PERIODS
45Å $N_D = 4 \times 10^{17} cm^{-3}$ (Si) GaAs
500Å x = 0.3 $Al_XGa_{1-X}As$ UNDOPED
0.5μm GaAs $N_D = 4 \times 10^{17} cm^{-3}$ (Si)
300Å $Al_XGa_{1-X}As$ x = 0.3 STOP - ETCH $N_D = 4 \times 10^{17} cm^{-3}$
DOUBLE SIDED POLISHED
3" SEMI-INSULATING GaAs

Fig.

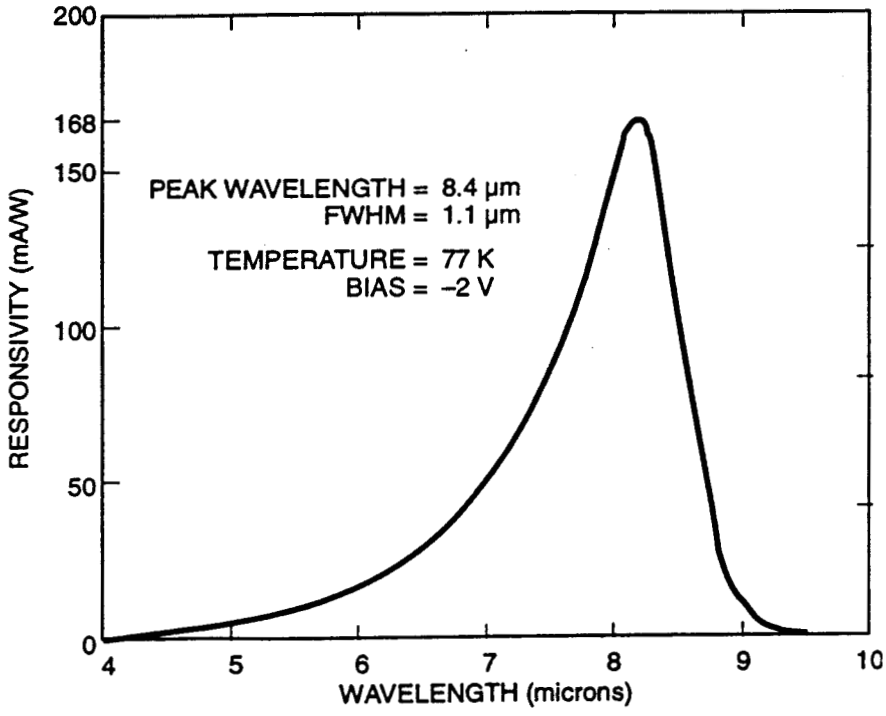
200
168
150
100
50
0
RESPONSIVITY (mA/W)
PEAK WAVELENGTH = 8.4 µm
FWHM = 1.1 µm
TEMPERATURE = 77 K
BIAS = –2 V
4
5
6
7
8
9
10
WAVELENGTH (microns)

Fig.

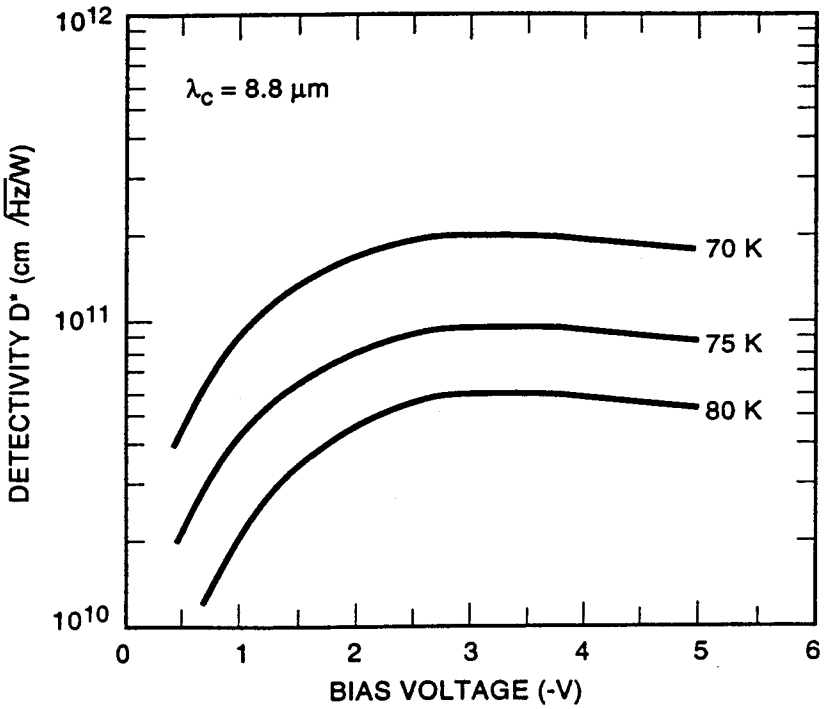
10^{12}
10^{11}
10^{10}
λ_c = 8.8 μm
70 K
75 K
80 K
DETECTIVITY D* (cm √Hz/W)
0
1
2
3
4
5
6
BIAS VOLTAGE (-V)

Fig

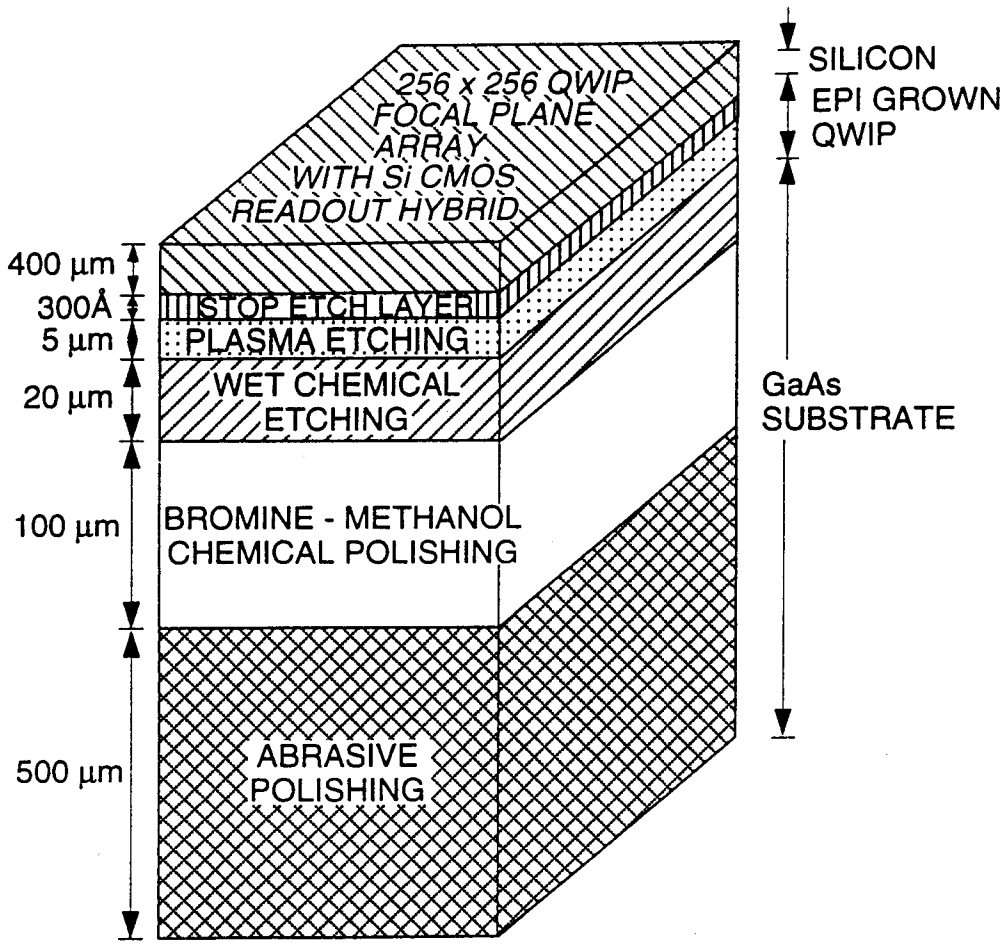
256 x 256 QWIP
FOCAL PLANE
ARRAY
WITH Si CMOS
READOUT HYBRID
SILICON
EPI GROWN
QWIP
400 µm
300Å
STOP ETCH LAYER
5 µm
PLASMA ETCHING
20 µm
WET CHEMICAL
ETCHING
GaAs
SUBSTRATE
100 µm
BROMINE - METHANOL
CHEMICAL POLISHING
500 µm
ABRASIVE
POLISHING

Fig

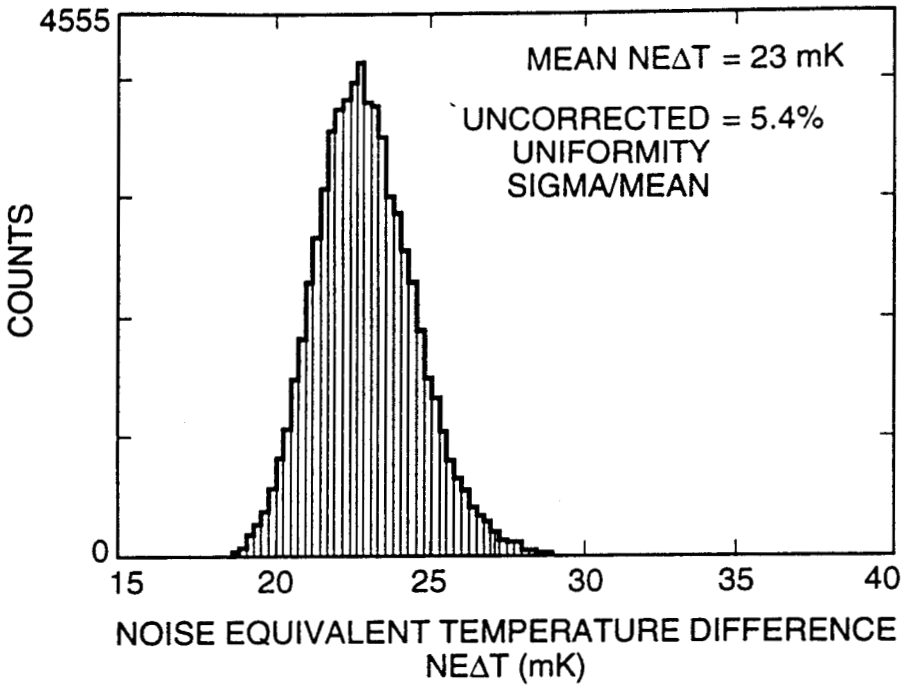
4555
0
COUNTS
MEAN NEΔT = 23 mK
UNCORRECTED = 5.4%
UNIFORMITY
SIGMA/MEAN
15
20
25
30
35
40
NOISE EQUIVALENT TEMPERATURE DIFFERENCE
NEΔT (mK)

Fig

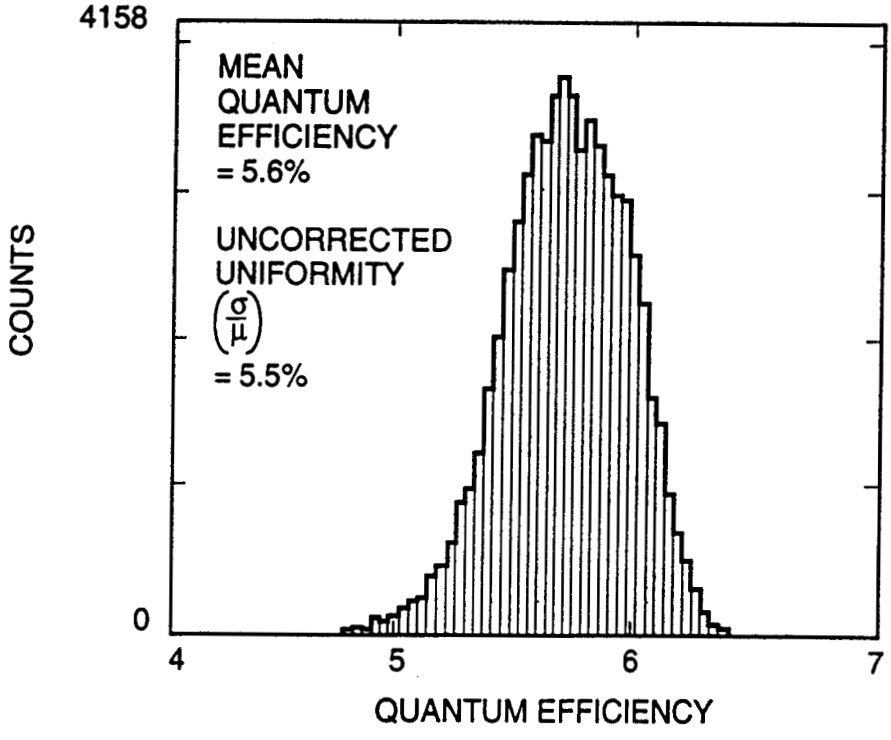
4158
MEAN
QUANTUM
EFFICIENCY
= 5.6%
UNCORRECTED
UNIFORMITY
$\left(\frac{\sigma}{\mu}\right)$
= 5.5%
COUNTS
0
4
5
6
7
QUANTUM EFFICIENCY

Fig.

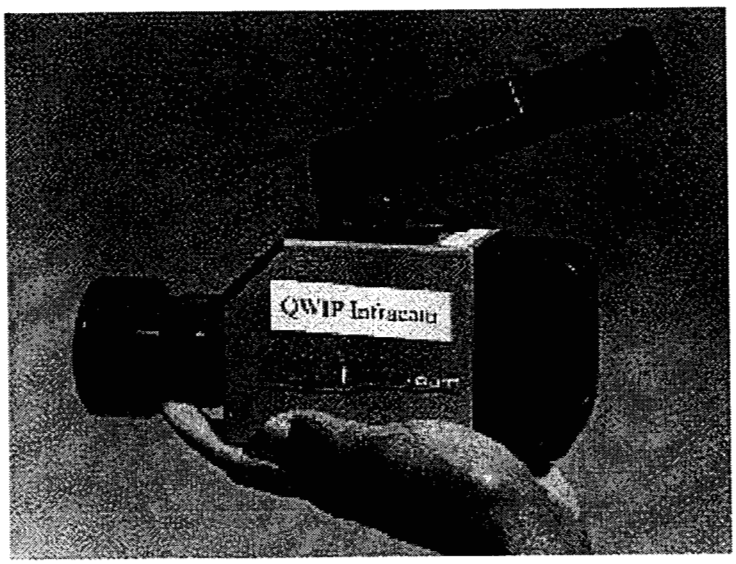
QWIP Infrared

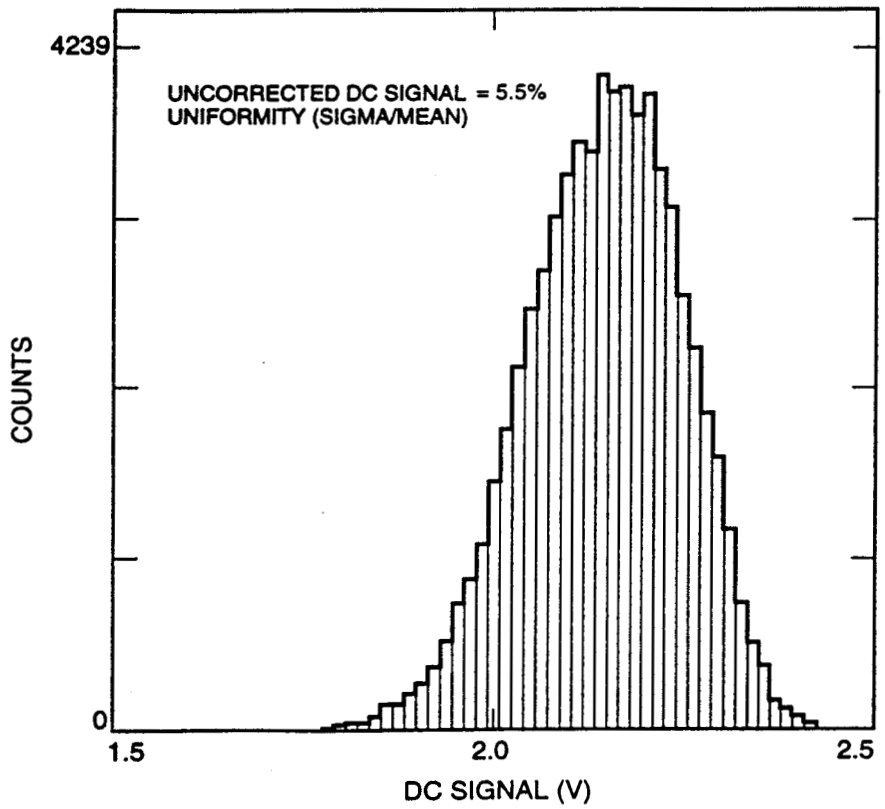
4239
UNCORRECTED DC SIGNAL = 5.5%
UNIFORMITY (SIGMA/MEAN)
COUNTS
0
1.5
2.0
2.5
DC SIGNAL (V)

Fig.

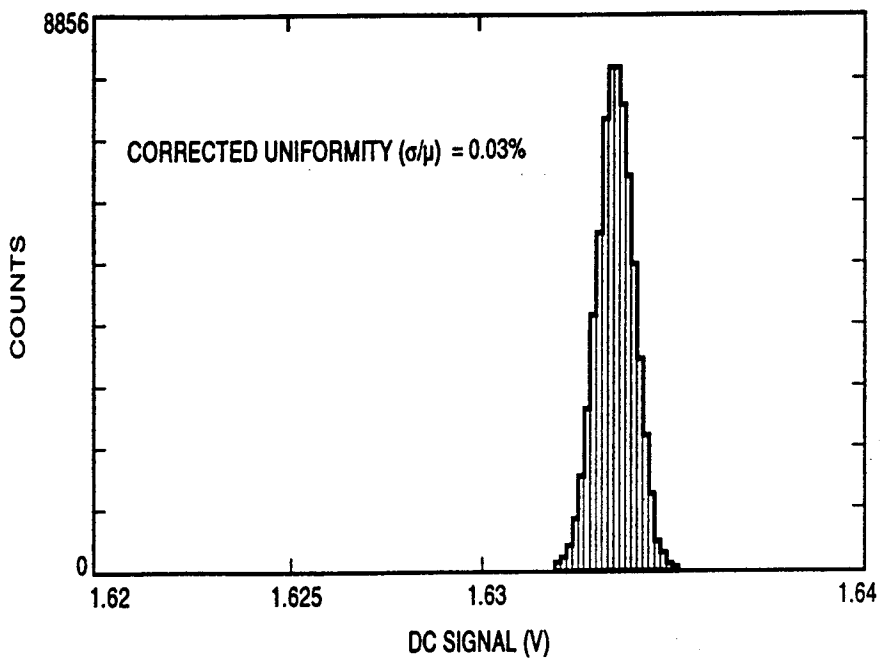
8856
CORRECTED UNIFORMITY (σ/μ) = 0.03%
COUNTS
0
1.62
1.625
1.63
1.64
DC SIGNAL (V)

Fig

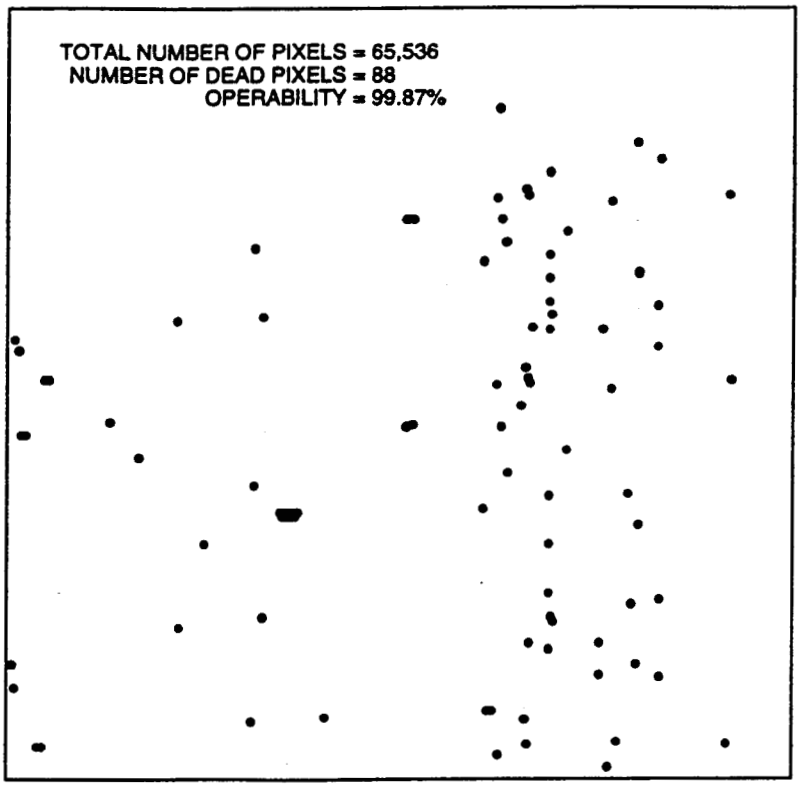
TOTAL NUMBER OF PIXELS = 65,536
NUMBER OF DEAD PIXELS = 88
OPERABILITY = 99.87%

Fi

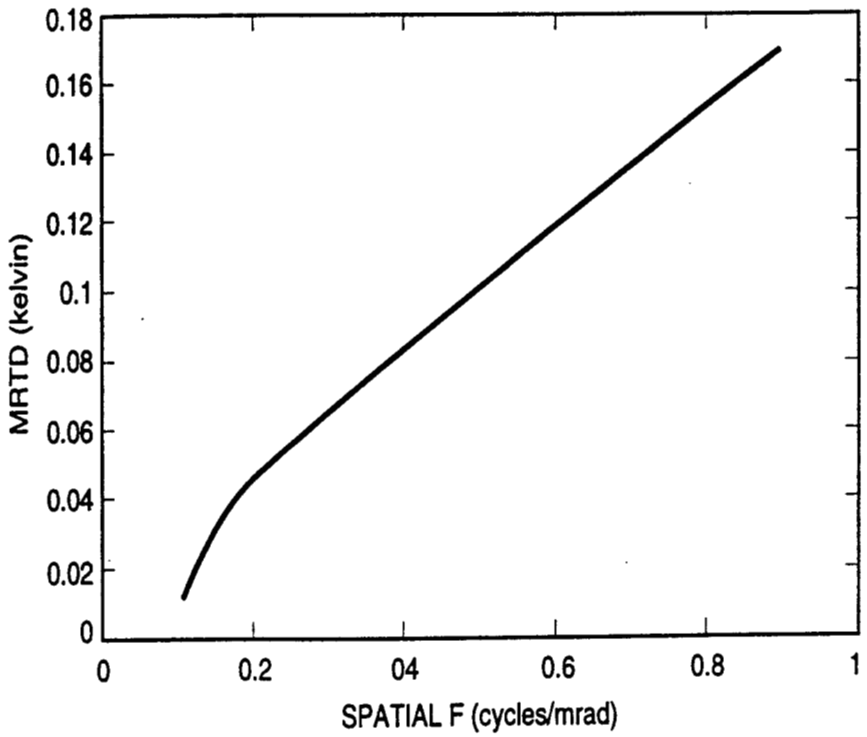
0.18
0.16
0.14
0.12
0.1
0.08
0.06
0.04
0.02
0
MRTD (kelvin)
0
0.2
04
0.6
0.8
1
SPATIAL F (cycles/mrad)

Fig.